nature communications

Article

https://doi.org/10.1038/s41467-025-64664-9

Biomimetic self-reinforcing recyclable biomass-derived inherently-safe sustainable materials

Received: 27 March 2025

Accepted: 19 September 2025

Published online: 03 November 2025

Check for updates

Rui-Zhi Wu, Xing-Liang Li ✉, Huan-Sheng Cai, Ning Zhao, Fu-Gui Wang, Ke-Rui Ye, Xiu-Li Wang, Yu-Zhong Wang & Teng Fu ✉

Biomass-derived recyclable materials that can replace petrochemical-derived plastics are highly sought for a sustainable future. However, incumbent materials often face performance deterioration challenges owing to the aging issues after use in the environment. Here, we present a self-reinforcing, recyclable, unprecedented polyester material derived entirely from biomass lignin and soybeans, mimicking the self-reinforcement mechanism of biological systems. Our material leverages a [2 + 2]-cycloaddition reaction mediated by aromatic π-conjugated vinylidene structures, enhancing performance under ultraviolet light, hygrothermal conditions, and external electric fields. Specifically, the tensile strength, elongation at break, and anti-ultraviolet efficiency can be enhanced to 103 MPa, 560%, and 73%, respectively, far surpassing those of known biomass-derived materials and engineered plastics. Additionally, the material demonstrates outstanding insulativity, barrier properties, flame retardancy, solvent resistance, and recyclability, meeting the demands of sustainable green new energy material. Our strategy for this self-reinforcing biomass recyclable material provides rich possibilities for designing next-generation sustainable materials.

The development of sustainable materials is gaining momentum as part of global efforts to reduce pollution and dependence on petroleum plastics, aiming to provide eco-friendly alternatives and minimize environmental impact[1–3]. Biomass-derived polymers have gained attention for their environmental advantages, including lower carbon footprints, sustainability, and the potential for tailored designs to improve recyclability[4–6]. These attributes position biomass-derived polymers as promising candidates for sustainable materials to address the resource and environmental issues[7]. However, incumbent polymer materials (polyethylene terephthalate[8], polyolefins[9], epoxy resin[10], etc.) degrade chemically or physically when exposed to ultraviolet (UV) radiation[11], external electric fields[12], or hygrothermal environments[13], reducing their performance and lifespan. While additives like UV absorbers can enhance durability, they often compromise mechanical properties and pose health and environmental hazards due to migration from the polymer matrix[14–17]. Additionally, the lack of effective end-of-life solutions for these aging materials leads to significant environmental concerns. Therefore, addressing the aging and sustainability of these polymers remains a daunting issue[18,19].

The human body provides a compelling model for addressing aging[20]. While aging is an inevitable process for all biological organisms, human biological systems employ advanced self-regulation mechanisms to repair and renew cell tissues, where regular use triggers metabolic processes that rebuild and strengthen tissues, enabling them to become stronger with use, counteracting the effects of aging[21]. As a result, people have long been fascinated by the anti-aging capability of biological systems. Mimicking the strategies of the biological systems represents a feasible way to develop sustainable materials that

State Key Laboratory of Advanced Polymer Materials, Polymer Research Institute, Collaborative Innovation Center for Eco-Friendly and Fire-Safety Polymeric Materials (MoE), National Engineering Laboratory of Eco-Friendly Polymeric Materials (Sichuan), Sichuan University, Chengdu, China.
✉e-mail: xingliangli@scu.edu.cn; futeng@scu.edu.cn

are self-reinforced and resistant to aging[22]. By drawing inspiration from cellular metabolic mechanisms in biological systems, it is possible to design materials that can self-repair and resist aging through the cleavage and reconfiguration of internal bonds, similar to the body's own response to wear and tear[23].

We developed a self-reinforcing, biomass-derived sustainable polyester material (PAOM) that combines exceptional performance with chemical recyclability. This material demonstrates remarkable performance enhancement behavior under UV radiation, external electric fields, and hygrothermal environments by mimicking the body's anti-aging mechanisms (Fig. 1). Our findings hinge on the physical and chemical cross-linking network facilitated by a [2 + 2]-cycloaddition reaction[24] triggered under service conditions, driven by the aromatic π-conjugated vinylidene structure of a hydroxyethylated soy isoflavone monomer (DDF–OH)[25]. This innovative design allows the material to resist the aging typically caused by environmental factors (UV radiation, external electric fields, and hygrothermal conditions)[23], significantly enhancing its tensile strength (103 MPa), elongation at break (560%), and anti-UV efficiency (73%), showing improvements of 61%, 201%, and 9%, respectively, far exceeding the performance of existing biomass-derived materials and engineered plastics. Additionally, PAOM exhibits superior barrier properties[26], flame retardancy, and solvent resistance compared to petrochemical-based materials, meeting the demands of sustainable energy solutions. Its unique ester bond structure enables low-temperature depolymerization, allowing for the recovery of polymerized monomers that can be re-polymerized to create new-generation materials or high-performance adhesives[27–31], achieving a maximum adhesion strength of 1.7 MPa comparable to traditional strong adhesives. Our work on self-reinforcing biomass-derived sustainable material, potentially driving the rapid development of more environmentally friendly and sustainable materials science.

Results

Biomimetic principle, fabrication, and structure

Biological systems exhibit remarkable self-reinforcing anabolic mechanisms, enabling them to resist aging and maintain functionality through cycles of tissue damage and reconstruction[32]. These mechanisms served as the inspiration for the design and preparation of the biomass-derived sustainable materials with similar properties[33]. To emulate this process, we design a biomass-derived material that incorporates self-reinforcement through a [2 + 2]-cycloaddition reaction, facilitated by the aromatic π-conjugated vinylidene structures in DDF–OH (Fig. S2A–D, Table S1). Subsequently, we utilize abundant biomass feedstocks, including DDF–OH, dimethyl furan-2,5-dicarboxylate (DMFD), and 1,4-butanediol (BDO)—to craft the material through a simple melt polymerization process (PAOM-1 to PAOM-4 denote the progressive increase in the content of DDF–OH, Fig. S6–S10, Table S2). The resulting material (PAOM) demonstrates a self-reinforcing mechanism akin to those in biological systems. Specifically, the cycloaddition reaction of the double bonds in DDF–OH, along with π-π stacking interactions, mimics the tissue damage-and-reconstruction process, ultimately enhancing the material's overall performance. (Fig. 1).

The π-π stacking interactions and reduction in free volume introduced by the rigid DDF–OH are pivotal to achieving the high-performance biomass-derived sustainable materials. Our X-ray diffractometer (XRD) analysis confirms the π-π stacking interactions within DDF–OH (Fig. 2A), with diffraction peaks at 2θ angles of 29.6° and 33.2°, corresponding to d-values of 0.32 nm and 0.28 nm, respectively, typical of aromatic π-π stacking distances[34]. By facilitating these interactions, DDF–OH reduces the free volume in PAOM, forming a physically cross-linked network that increases chain segment friction, enhances molecular dynamic volume, and promotes tighter molecular packing. This network strengthens intermolecular forces, improving the material's rigidity and overall performance[35]. We corroborated our theoretical insights from correlation analyses using low-field nuclear magnetic resonance (NMR) measurements, melt rheology characterization, dynamic thermomechanical analysis (DMA), positron annihilation lifetime spectrum (PALS), and molecular dynamics simulation (MD). Low-field NMR measurements unveil a decrease in relaxation time to 0.08 ms with the introduction of DDF–OH (Fig. 2B, C). Simultaneously, melt rheology tests reveal an increase in complex viscosity (η), storage (G'), loss (G''), and zero shear viscosity (η_0) as DDF–OH content increases (Figs. 2D–G, S11). DMA confirms a promotion in tensile storage modulus with higher DDF–OH, indicating enhanced chain segment friction and molecular dynamic volume. (Fig. 2H) PALS further characterizes the free volume, showing a decrease in the corresponding o-Ps (I_3, according to the free volume theory; detail equations can be found in the supplementary information and Table S5) and the fractional free volume (FF_V) from 10.49% to 9.65% and 0.99% to 0.89%, respectively, with increasing DDF–OH content. Subsequently, the π-π stacking interaction and the free volume (F_V) of PAOM are calculated by MD. The distance between the two benzene rings in DDF is 3.53 Å, consistent with the typical π-π stacking distance, confirming the presence of π-π interactions

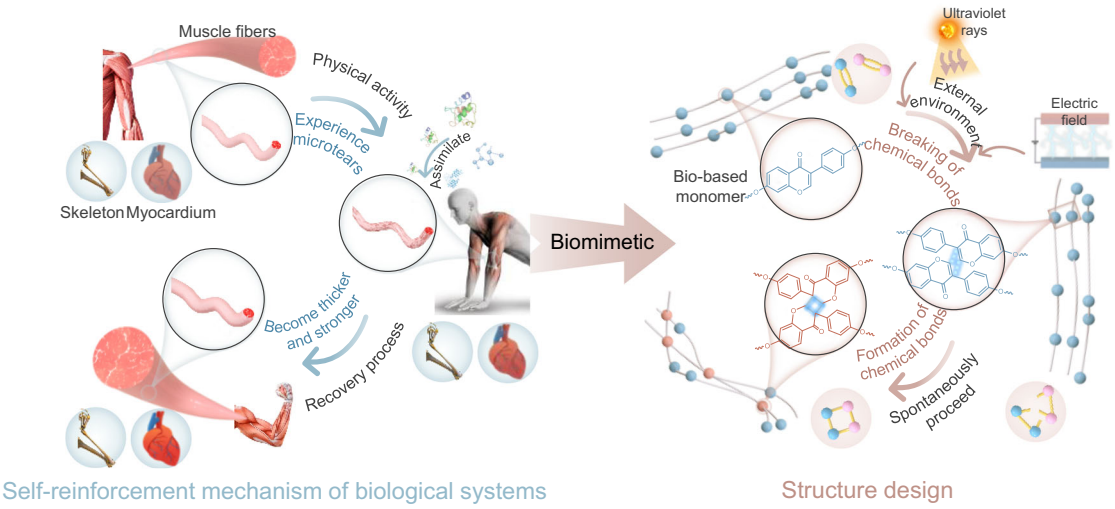

Fig. 1 | Schematic illustration of biomimetic strategies. Schematic illustration of biomimetic strategies for self-reinforcing recyclable biomass-derived materials.

https://doi.org/10.1038/s41467-025-64664-9

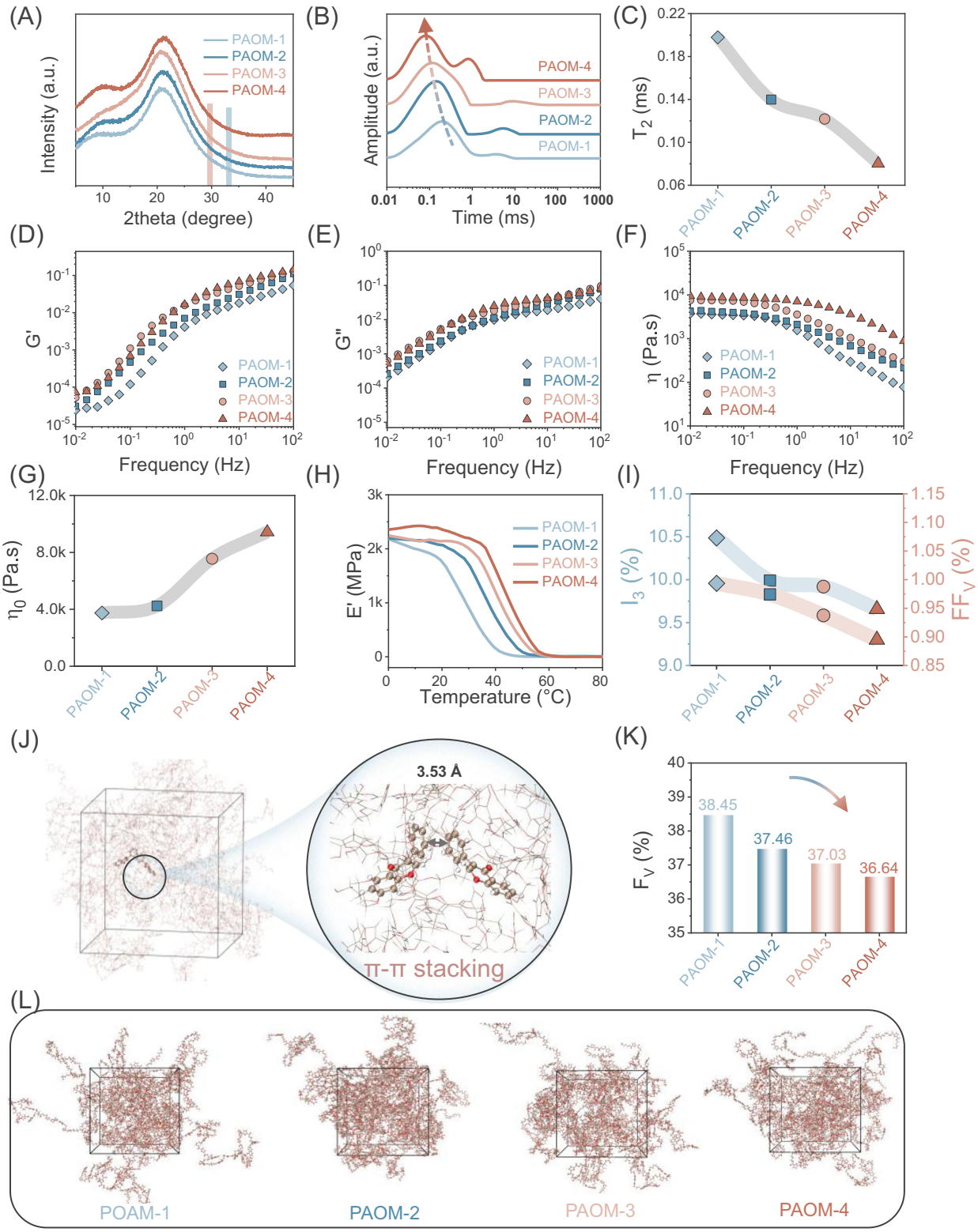

Fig. 2 | Structural characterization of PAOM. A XRD pattern of PAOM. **B**, **C** Low-field NMR curves and transverse relaxation time (T_2) distribution curves, the shaded area in the figure represents the trend of the parameter variation with increasing incorporation level. **D**–**G** Frequency-dependent curves of G', G'', η, η_0 for PAOM, the shaded area in the figure represents the trend of the parameter variation with increasing incorporation level. **H** Temperature-dependent storage modulus (E') curve of the polymer. **I** Positron lifetime analysis for PAOM. **J**–**L** Molecular dynamics (MD) simulations revealing the internal π-π stacking, fractional free volume, and molecular chain models of the material.

(Fig. 2I)[34]. The simulations also reveal a decrease in F_V from 38.45% to 36.64%, driven by increased chain stiffness and tighter molecular packing (Fig. 2K–L). This reduction in free volume significantly improves the mechanical and functional properties of PAOM.

Multifunction of PAOM

The π-π stacking interactions formed by rigid DDF–OH units, combined with the resulting small free volume, impart PAOM with exceptional multifunctionality in terms of crystallinity, heat resistance, mechanical strength, barrier properties, solvent resistance, and flame retardancy. We examine the crystallization and thermal stability through differential scanning calorimetry (DSC), XRD, and thermogravimetric analysis (TGA). TGA tests reveal the resulting polymers are thermally stable, with high decomposition temperatures at 5% weight loss (T_{d5} = 348 °C to 355 °C), maximum decomposition temperatures (T_{max} = 385 °C to 389 °C), and the residual mass (R_{700} = 5.5% to 10.9%) (Fig. S12, Table S3). Increasing DDF–OH content results in a slight decrease in crystallinity (21.4% to 18.1%), while the glass transition temperatures (T_g) rise from 45 °C to 55 °C (Fig. S13, 14, Table S3). Meanwhile, the optical properties also vary with DDF–OH content. As its proportion increases, the optical transparency of the films decreases slightly from 88.3% to 82.9%, accompanied by an increase in haze values from 9.4% to 22.4% (Fig. S15).

Mechanical properties, barrier performance, solvent resistance, and flame retardancy are critical for sustainable materials. Achieving multiple excellent properties simultaneously is challenging, yet our PAOM materials stand out in this regard because the physical cross-linking network created by the π-π stacking interaction enhances chain entanglement and molecular rigidity. Our stress-strain analyses reveal significant improvements in strength and toughness (Fig. 3A– C, Table S6), with young's modulus (E) and tensile strength (σ) increasing by 28% and 12%, respectively, as DDF–OH content rises (E = 975.5 MPa (PAOM-1) to 1091.0 MPa (PAOM-4); σ = 50.0 MPa (PAOM-1) to 64.0 MPa (PAOM-4)). Furthermore, all samples also demonstrate excellent extensibility, with the tunable strain at break (ε_b) ranging from 186.3% to 386.3%. Notably, PAOM-1 and PAOM-2 exhibit strains exceeding 360.0%, comparable to commercial PI[36] and surpassing many engineering plastics (Table S6)[37–44]. Our gas manometric technique depicts the excellent barrier performance of the PAOM (Fig. 3D–F)[45]. CO_2, O_2 and H_2O permeability coefficients unveil a decreasing (1.81×10^{-5} to 1.23×10^{-5} barrer, 2.46×10^{-5} to 1.30×10^{-5} barrer, and 1.51×10^{-14} to 1.30×10^{-14} g·cm/(cm^2 s Pa), respectively) as the content of DDF–OH increases, attributing to reduced free volume and tighter molecular packing from π-π interactions. These results show that the PAOM films offer superior barrier performance compared to many biomass-based and engineering plastics (Fig. 3G), supporting their suitability for green energy systems and potential broader engineering applications (Table S7)[46–50]. The polyesters also demonstrate excellent solvent resistance, maintaining their shape and weight after immersion in various organic solvents for seven days (Figs. 3H, S16, 17 and Table S8). Regarding the fire safety of the PAOM, it boasts a substantial limiting PHRR and THR of 544.6–460.3 W/g and 19.1–16.9 kJ/g, unveiling a 15.5% and 11.5% reduction in PHRR and THR as DDF–OH content increases, signifying its incapability to sustain continuous combustion under typical conditions (Fig. 3I, J). This is attributed to char formation facilitated, which limits oxygen exposure and inhibits sustained combustion[51], providing excellent flame-retardant properties. The multifunctionality of PAOM polyesters—combining thermal stability, mechanical strength, barrier performance, solvent resistance, and flame retardancy—makes them ideal candidates for green energy systems. Their durability and safety features also position them as promising candidates for broader engineering applications, ensuring long service life under challenging environmental conditions.

Insulation properties of PAOM

Building on their excellent mechanical strength, barrier performance, and flame retardancy, we explore the potential of PAOM in green power applications, particularly for its insulation properties. Hopping conduction is identified as the dominant charge transport mechanism in dielectric materials, which is influenced by localized states or "traps". These traps, which enhance the material's insulating capabilities, arise from the differences in molecular orbital (LUMO, HOMO) energy levels (Φ_e, ΔE) between neighboring molecular chain segments[52], as depicted in Fig. 4A[53,54]. Our density functional theory (DFT) calculations confirm that introducing the DDF–OH structure (Fig. 4B) significantly alters the π-conjugated system in structural unit B (containing DDF–OH and FDCA units). Compared to structural unit A (containing FDCA and BDO units, HOMO: −7.28 eV, LUMO: −2.47 eV), unit B exhibits a higher HOMO energy level (−6.23 eV) and a lower LUMO energy level (−2.69 eV), resulting in an electron trap depth (φ_e) of 0.22 eV and a lower HOMO-LUMO energy gap (ΔE: 3.51 eV vs. 4.81 eV for unit A). These characteristics restrict electron movement, thereby enhancing the insulating properties of PAOM. We further corroborate our theoretical insights from correlation analyses using space charge tests (Fig. S18)[55]. During the polarization process, charges are injected into the polymer from both the positive and negative electrodes via Fowler–Nordheim tunneling, a field-induced injection mechanism that dominates under high electric field conditions, with both the charge density and electric field strength increasing over time. The introduction of DDF–OH reduces charge migration and accumulation. After 15 min of polarization, the electric field strength of PAOM-4 (8.0 kV/mm) is 69.6% of that of PAOM-1 (11.5 kV/mm). After 30 min, a negative charge concentration region forms within PAOM, and the charge density difference between regions decreases with increasing DDF–OH content (Fig. 3E). This indicates more traps in PAOM-4, further obstructing charge migration. During depolarization, the trapped charges gradually migrate to the surface. Even after 30 minutes, PAOM-4 maintains a higher internal charge concentration (1.22 C/m^3) than materials with lower DDF–OH content (Fig. 3F), indicating reduced charge mobility and higher resistivity. The increased trap density also inhibits secondary impact ionization, enhancing breakdown strength and preventing material degradation[56]. Consequently, the surface resistivity and breakdown strength of PAOM improve with higher DDF–OH content. PAOM-4 achieves a surface resistivity of 3.91×10^{13} Ω/cm and a breakdown strength of 67.56 kV/mm, representing a 1600% increase in resistivity and a 51% increase in breakdown strength compared to PAOM-1 (Fig. 4G, H). These results underscore the suitability of bio-based PAOM materials for sustainable green power systems.

Sustainability of PAOM: self-reinforcing and closed-loop recycling

Conventional materials often age under external environments like UV radiation, hygrothermal conditions, and electric fields, leading to safety hazards and significant waste disposal challenges, rendering them unsuitable for sustainable development. In contrast, PAOM offers remarkable sustainability across its entire lifecycle, originating from renewable biomass lignin and soybeans, and featuring self-reinforcing capabilities during use with recyclability after disposal, an ideal sustainable material. A key innovation of PAOM is the incorporation of the biomass-derived DDF–OH monomer, whose aromatic π-conjugated vinylidene structure draws inspiration from biological self-reinforcement mechanisms. The cycloaddition reactions and π-π stacking interactions in PAOM enhance its mechanical properties and provide UV resistance (Figs. 5A, S19). Our DFT calculations confirm that the DDF–OH cycloaddition creates a stable π-conjugated system with a four-membered ring (Fig. 5B). This structure lowers the unoccupied molecular orbital (LUMO) energy level to -1.81 eV and narrows the

https://doi.org/10.1038/s41467-025-64664-9

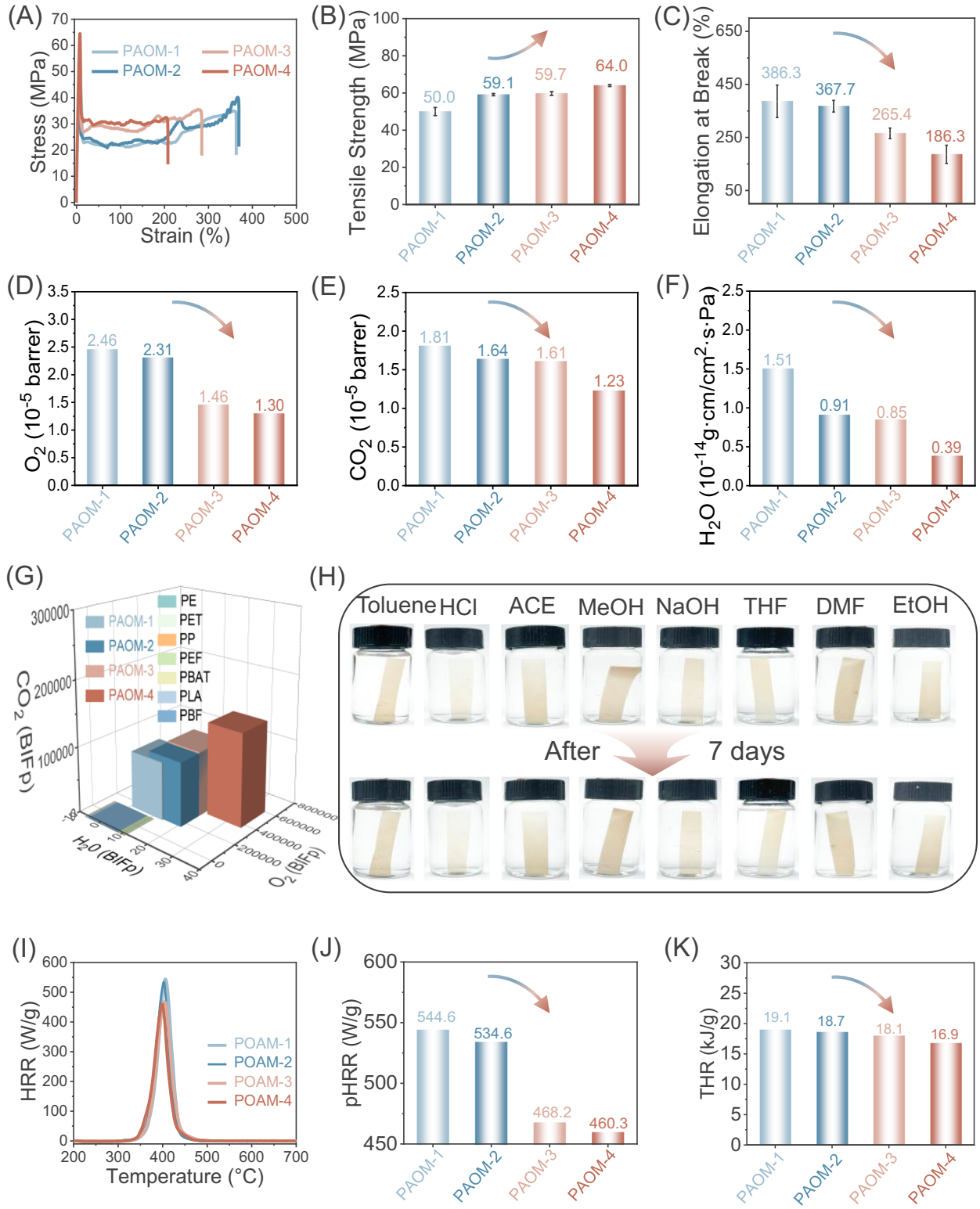

Fig. 3 | Mechanical properties, barrier properties, solvent resistance, and flame retardancy of PAOM. A–C Stress–strain curves, tensile strength, and elongation at break of PAOM. The bar represents the mean value for three individual experiments, and the error bar is s.d. based on three individual experiments. **D–G** Composition dependence of CO_2, O_2, and H_2O barrier properties of PAOM, along with a comprehensive comparison of gas barrier performance between PAOM-4 and other materials[46–50]. **H** Solvent resistance of PAOM-4 films. **I–K** Heat release rate (HRR), peak heat release rate (pHRR), and total heat release (THR) of PAOM.

https://doi.org/10.1038/s41467-025-64664-9

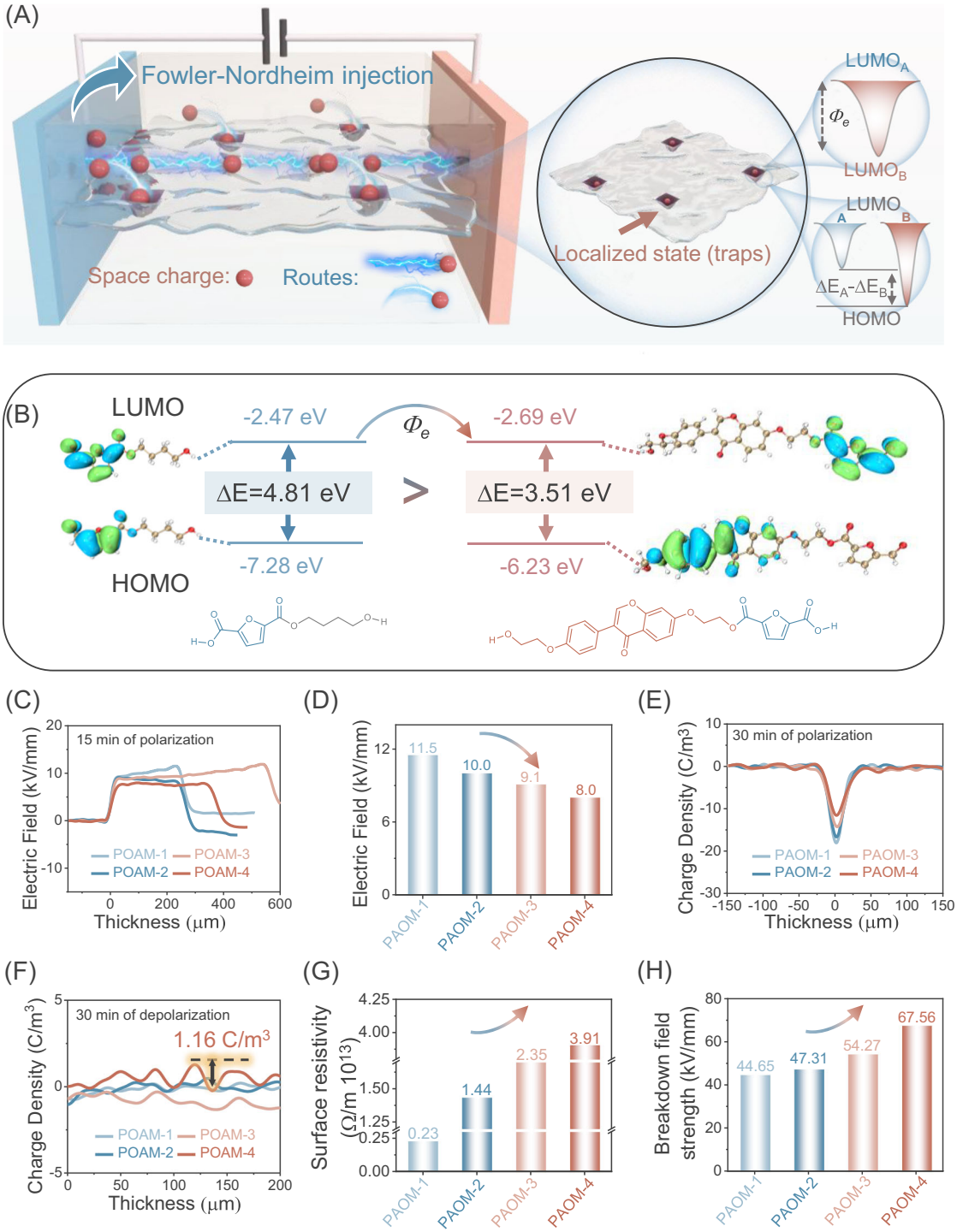

Fig. 4 | Insulation properties of PAOM. A Schematic diagram of the insulation mechanism. **B** Molecular orbital energy of different units. **C**, **D** Electric field intensity distribution and maximum electric field intensity inside PAOM after polarization for 15 min in the space charge test. **E** Charge density on the surface of PAOM after polarization for 30 min. **F** Charge density inside PAOM after depolarization for 30 min. **G**, **H** Surface resistivity and breakdown field strength of PAOM.

HOMO-LUMO energy gap (ΔE: 4.11 eV) compared to DDF–OH (LUMO: −1.63 eV, ΔE: 4.25 eV), improving material stability. These changes result in PAOM's enhanced UV resistance, mechanical properties, and durability under external environmental conditions. PAOM efficiently blocks UV-B rays (280–320 nm) and filters 67% of UV-A rays (320–400 nm), outperforming widely used power materials like polyethylene[57] and polyethylene terephthalate[58], which allow more than 80% UV transmission (Fig. 5C). Tests with a digital UV light meter reveal that PAOM films can reduce UV intensity by up to 96.9% (10.23 mW cm^{-2} without the film, 3.84–0.32 mW cm^{-2} after covering with the PAOM film, Fig. 5D). Remarkably, after three hours of intense UV irradiation—equivalent to 51 years of natural sunlight at a UV index of 8 (the annual average UV index in Chengdu, China, is 7 to 9[59], Fig. S11; detailed calculations are provided in the supplementary materials)—PAOM exhibits significant improvements in UV resistance and mechanical properties. Its transparency increases by up to 12%

https://doi.org/10.1038/s41467-025-64664-9

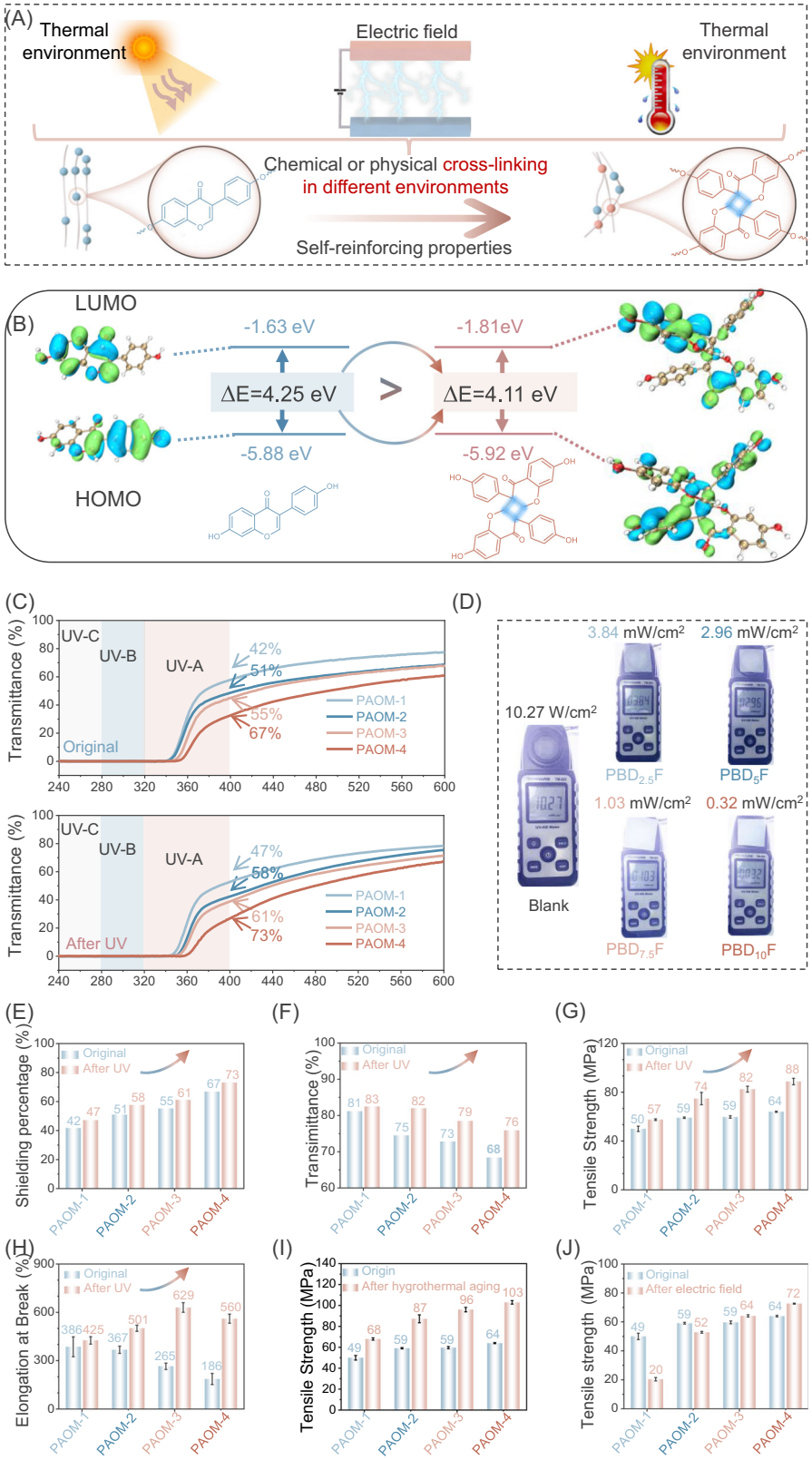

Fig. 5 | Self-Reinforcing behavior of PAOM. A Schematic diagram of the self-reinforcement mechanism of PAOM. **B** Optimized molecular geometries and HOMO–LUMO energy levels for DDF (left) and photo-crosslinked system (right) by density functional theory calculation. **C** UV transmittance of PAOM films before and after UV irradiation (thickness: 0.3 mm). **D** UV resistance testing of PAOM under UV lamp. **E**, **F** Shielding efficiency at 400 nm and transmittance at 750 nm for both original and UV-irradiated films. **G**, **H** Tensile strength and elongation at break of original and UV-irradiated PAOM films. The bar represents the mean value for three individual experiments, and the error bar is the standard deviation based on three individual experiments. **I**, **J** Tensile strength of PAOM films and those after hygrothermal aging and electric field. The bar represents the mean value for three individual experiments, and the error bar is the standard deviation based on three individual experiments.

from 76–83%, and UV-A shielding efficiency increases by 9–14%, reaching up to 73% (Fig. 5E, F). Additionally, tensile strength rises from 57 MPa to 88 MPa, while elongation at break increases from 425% to 629%, reflecting substantial gains in both strength and flexibility (Figs. 3D–H, S20). Regarding the self-reinforcing performance of PAOM in a hygrothermal environment (60 °C, 99% RH for 100 h, Fig. 3I), it maintains impressive mechanical properties, with tensile strength increasing by 39–63%, reaching values from 68 MPa to 103 MPa. Similar to the changes in mechanical properties under a hygrothermal environment, materials with higher DDF–OH content retain their tensile strength under high voltage (10 kV for 30 min), reaching up to 72 MPa, a 13% increase (Fig. 3J). However, materials with lower DDF–OH content (2.5–5 mol%) are insufficient to counteract voltage-induced degradation, resulting in lower tensile strengths (20–52 MPa). Despite slight reductions in elongation at break under electric field or hygrothermal conditions, PAOM continues to meet the required performance standards for practical use (Fig. S21). These enhancements in durability and self-reinforcing properties stem from PAOM, the formation of "locked" interchain crosslinks through cycloaddition reactions and π-π interactions, leading to better UV resistance and mechanical strength, far surpassing those of known biomass-derived materials and engineered plastics[35,37–44,60–62]. This makes PAOM an ideal, long-lasting, sustainable material, especially for green power systems.

After completing its service life, waste PAOM offers promising recycling and upcycling options that significantly enhance its sustainability[63–68]. PAOM's ester-functionalized polymer backbones enable effective recycling through cosolvolysis. The polyester PAOM can be completely depolymerized into its original monomers via a low-temperature (90 °C) chemical recycling process. Using a co-solvent system (EtOH/BDO) and a cost-effective NaOH catalyst, we achieve a high purity and high yield (83%) of DDF–OH (rDDF–OH), which appears as a light-yellow precipitate. (^{1}H NMR, Figs. S22, 23). Further treatment with HCl yields recycled FDCA (rFDCA), a white precipitate with a purity of 99.0% and a yield of 91.0%. This rFDCA is then methyl-esterified to obtain recycled DMFD (rDMFD) with a purity exceeding 99.0%, as confirmed by FTIR, ^{1}H NMR, ^{13}C NMR, and LC analysis (Figs. S24–29). The residual solution is distilled at 80 °C to remove EtOH, and vacuum distilled at 140 °C to recover recycled BDO (rBDO) with a purity of 99.8%, surpassing standard BDO purity (Figs. S30–32).

We propose two sustainable pathways for reusing these monomers: repolymerization and upcycling. The first involves repolymerizing rDDF–OH, rDMFD, and rBDO into the second generation of polyester, rPAOM-4. Structural analyses by ^{1}H NMR confirm the successful synthesis of rPAOM-4 (Fig. S33), which exhibits mechanical properties nearly identical to the original PAOM-4 (Fig. 6H, I). Structural analysis by ^{1}H NMR confirms the successful synthesis of rPAOM-4 (Fig. S23), which exhibits mechanical properties nearly identical to the original PAOM-4, with a tensile strength retention of 96.9% and an elongation at break retention of 92.5% (Figs. 6H, I, S34, 35). The second pathway focuses on upcycling recovered monomers into polyurethane (up-PU) adhesives. Using biomass-derived rDDF–OH, rFDCA, polylactide diol, 2-ethyl-2-(hydroxymethyl)-1,3-propanediol (TMP), and isophorone diisocyanate (IPDI), we synthesize up-PU, with its structure confirmed by FTIR (Figs. S4, 6J, K). Mechanical testing reveals a tensile strength of 66.2 MPa (Fig. S36), while adhesive tests. show bonding strengths of 0.98 MPa to stainless steel and 1.69 MPa to polyamide, comparable to commercial petroleum-based EVA (Fig. 6L)[69]. PAOM's raw materials, derived entirely from renewable biomass resources, eliminate dependence on fossil fuels. Its excellent mechanical, barrier, flame-retardant, and self-reinforcing properties ensure durability in outdoor applications as a polymer material. Recycling PAOM into polyester and upcycling it into biomass adhesives addresses waste disposal challenges while enabling high-value applications, supporting the sustainable development of polymer materials.

Discussion

We have developed a biomimetic strategy that mimics biological systems to develop sustainable polyester materials with resistant aging and self-reinforcement of performance under typical outdoor usage environments. This biomass polyester is prepared by condensation copolymerization of DDF–OH, DMFD, and BDO. The π-π stacking interactions and the "locked" interchain crosslinking from a [2 + 2]-cycloaddition reaction mediated by aromatic π-conjugated vinylidene structures provide these materials with exceptional UV resistance, mechanical strength, and performance under UV radiation, hygrothermal conditions, and electric fields. The UV-A shielding efficiency can increase by up to 14%, shielding 73% of UV-A. More notably, tensile strength and elongation at break are significantly enhanced by 61% and 100%, respectively—reaching 103 MPa and 629%. These improvements highlight the material's remarkable self-reinforcement capabilities. Crucially, our materials are entirely derived from renewable resources and also boast high insulativity, barrier properties, flame retardancy, solvent resistance, and recyclability. The biomass monomers can be fully recycled into polyesters through repolymerization or upcycled to produce biomass adhesives with superior bonding properties. This self-reinforcing, recyclable biomass material represents an important step in the development of sustainable materials.

Methods

Chemicals and materials

A list of all chemicals and materials can be found in the supplementary Information section 1.1.

Synthesis of monomers, synthesis and recycling of polyesters

All reaction processes can be found in the supplementary Information sections 1.2–1.3.

Characterization

The chemical structure of the PAOM, rFDCA, rDMFD, and rBDO were characterized using ^{1}H NMR and ^{13}C NMR spectroscopy. The ^{1}H NMR and ^{13}C NMR spectra were recorded on a Bruker AC-P 400 MHz NMR instrument and a MesoMR23-060H-I instrument (Shanghai, China). Deuterated trifluoroacetic acid (TFA) was used as the solvent for the copolyesters, while DMSO-d6 and D_2O were used for the monomers.

Low-field nuclear magnetic resonance (LF-NMR) spectra were recorded using a VTMR20-010V-I in situ variable temperature NMR analyzer.

The FT-IR spectra were obtained using a Nicolet 6700 spectrometer.

The intrinsic viscosity [η] of the PAOM was determined using a Ubbelohde viscometer. All samples were dissolved in a 50/50 (v/v) phenol/1,1,2,2-tetrachloroethane solution at 25 °C. The intrinsic viscosity of the polyesters was calculated according to Eq. (1).

$$[\eta] = \frac{[2(t/t_0 - \ln(t/t_0) - 1)]^{\frac{1}{2}}}{c} \quad (1)$$

c is the solution concentration, t is the flow time of the solution, and t_O is the flow time of the solvent. The reported values are the average of three measurements.

The Restrained Electrostatic Potential (RSEP) charges for all molecules were fitted using the Multiwfn software, and the top file was obtained using the Sobtop software. The initial molecular simulation files were generated using Packmol software, with the number of molecules set according to the specified ratios. Molecular dynamics simulations were performed using Gromacs 5.03 software, employing the OPLS-AA (Optimized Potentials for Liquid Simulations All-Atom) force field. Energy minimization was first carried out, followed by NPT ensemble simulation at 300 K using the Berendsen pressure coupling method to achieve system equilibration. The time step was set to

https://doi.org/10.1038/s41467-025-64664-9

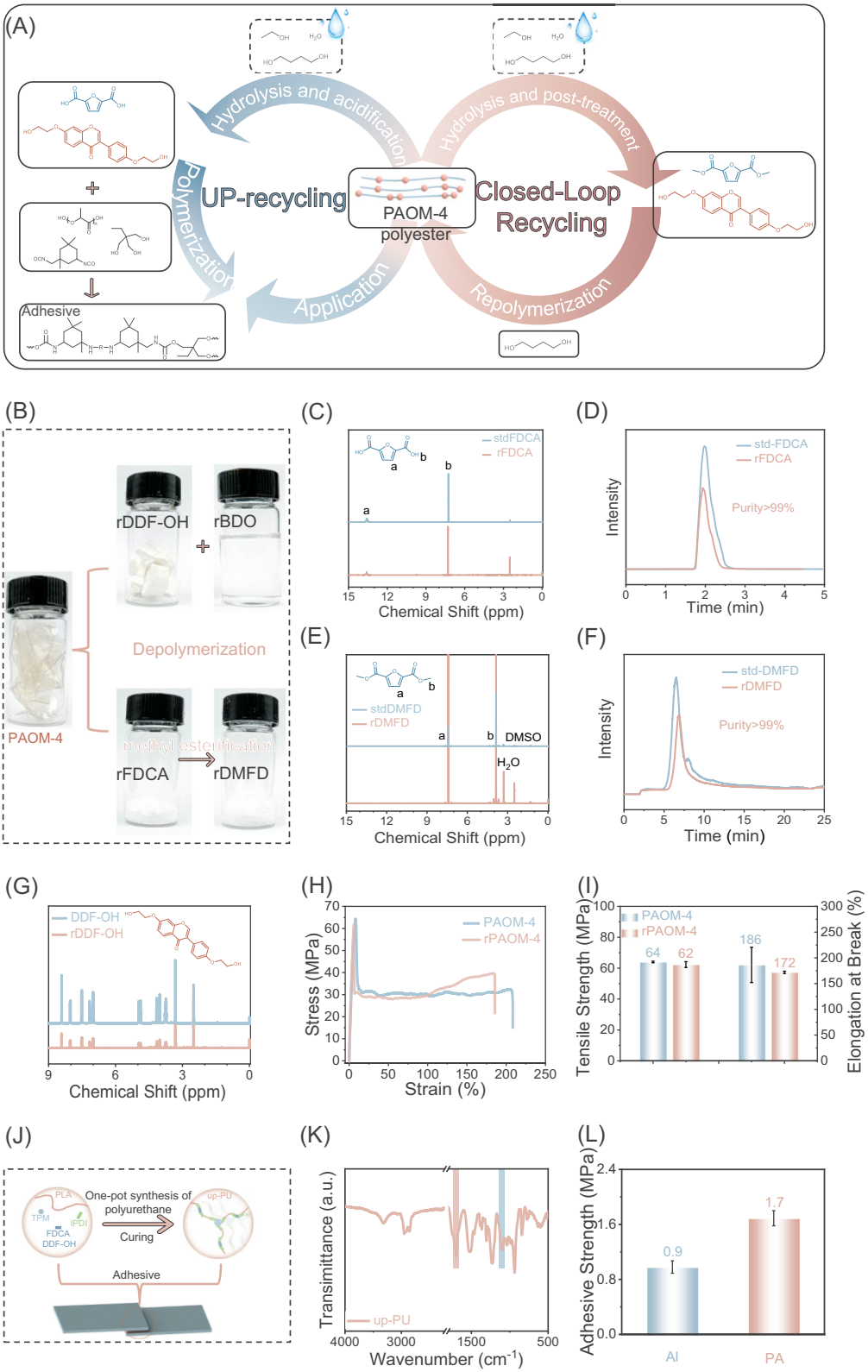

Fig. 6 | Chemical recycling of PAOM. A Schematic diagram of the recycling process of PAOM. **B** Digital photos of rDDF−OH, rBDO, rFDCA, and rDMFD obtained from the depolymerization of PAOM-4 in the H_2O/BDO/NaOH system. **C**–**F** ^{1}H NMR spectra in DMSO-d6 and LC analysis of FDCA/rFDCA and DMFD/rDMFD obtained from the recycling experiment. **G** ^{1}H NMR spectrum of rDDF−OH in DMSO-d6. **H**, **I** Stress–strain curves, tensile strength, and elongation at break of PAOM-4 and rPAOM-4. The bar represents the mean value for three individual experiments, and the error bar is the standard deviation based on three individual experiments. **J** Synthesis process of up-PU and its application as an adhesive. **K** FTIR spectrum of up-PU. **L** Adhesive strength of up-PU on Al and PA plates. The bar represents the mean value for three individual experiments, and the error bar is the standard deviation based on three individual experiments.

dt = 2 fs, with a total simulation time of 2 ns, and outputs were recorded every 1 ps. The Parrinello-Rahman pressure coupling method was then applied for an additional 2 ns NPT simulation. The temperature was then ramped up to 450 K for a 5 ns NPT simulation, and after that, a 10 ns NPT simulation was performed at 300 K to achieve system equilibrium. Finally, the v-rescale temperature coupling method was used for a 20 ns NVT ensemble simulation for production analysis, with all the figures obtained using VMD software.

Dynamic rheological tests were conducted using a Discovery HR-30 rheometer equipped with a 25 mm diameter parallel-plate geometry. Dynamic oscillatory shear measurements were performed across a frequency range of 0.01 to 100 Hz at 190 °C, under a strain of 1%, with a gap size of 1000 μm.

Differential scanning calorimetry (DSC) curves were acquired using a NETZSCH DSC 214 instrument. 5 mg of each sample was placed in alumina crucibles and scanned from 10 to 270 °C at a heating rate of 5 °C/min.

Thermogravimetric analysis (TGA) was performed using a NETZSCH TG 209 F1 thermogravimetric analyzer in a nitrogen atmosphere. Samples weighing 3–5 mg were heated from 40 °C to 700 °C at a rate of 10 °C/min.

The crystallinity of the copolyesters was characterized using wide-angle X-ray scattering (WAXS) on a Panalytical X'Pert MPD Pro diffractometer. The instrument utilized copper Kα1 radiation (λ = 1.5406 Å) and was equipped with an X'Celerator detector. The samples were scanned over a 2θ angle range of 5 ° to 45 °.

Positron annihilation lifetime spectroscopy (PALS) tests were conducted using a Finder1000 PALS system (model PLS-System). The positron source had a time resolution of 0.23 ns, and two small disks measuring 25 mm × 25 mm × 1 mm were placed between the ^{22}Na positron source. The positron lifetime was determined by measuring the time delay between the emission of one of the birth gammas (1.28 MeV) and the detection of the resulting 0.511 MeV annihilation photons.

The breakdown field strength of polyesters and copolyesters was assessed using a DDJ-50KV instrument, with the applied voltage ramped at a rate of 1 kV/s. The surface resistivity of the copolyesters was measured using an ST2742B instrument.

The micro combustion calorimetry (MCC) of the materials was evaluated using an FAA-PCFC instrument.

The mechanical properties of the copolyesters were evaluated using an Instron Universal Testing Machine (model 5567) at a crosshead speed of 5 mm/min at room temperature. Three specimens were tested for each sample, and the average result was reported.

The barrier properties to O_2 and CO_2 were analyzed using a manometric method with a Labthink VAC-V2 permeance testing device. The polyesters were prepared as circular disks with a thickness of 0.5 mm and a diameter of 50 mm. The gas permeability coefficient was recorded continuously until a stable permeability rate was achieved.

The UV-shielding properties of the copolyesters were evaluated using a Cary Eclipse spectrometer (Agilent, USA) at room temperature, across a wavelength range of 200–800 nm.

The hygrothermal aging test was conducted by placing the copolyester in a constant temperature and humidity chamber (ZH-TH-800) at 60 °C and 99% relative humidity for 100 h, followed by testing its mechanical properties.

The water absorption test was performed by placing the copolyester in a constant temperature and humidity chamber (ZH-TH-800) at room temperature (25 °C) and 99% relative humidity for 24 h, and then measuring the change in mass.

Space charge testing was conducted using a Japan-made Fivelab Peanuts instrument, with polarization for 30 min followed by depolarization for 30 min.

The purity of rFDCA, rDMFD, and rBDO was determined using liquid chromatography (LC) with a Finnigan TSQ Quantum mass spectrometer. The recycled liquid was analyzed using gas chromatography (GC) with an Agilent 7890B instrument, employing methanol as the solvent.

The solvent resistance of the copolyester films was assessed by immersing the samples in various solvents, including deionized water (H_2O), ethanol (EtOH), acetone (ACE), dimethyl sulfoxide (DMSO), methanol (MeOH), 5 wt% aqueous sodium hydroxide (NaOH), N, N-dimethylformamide (DMF), and tetrahydrofuran (THF), for 7 days at room temperature and pressure. The physical and chemical changes in the samples were then compared before and after exposure to these solvents.

Data availability

Source Data are provided with this paper. All other data are available from the corresponding author upon request. Source data are provided with this paper.

References

1. Stegmann, P., Daioglou, V., Londo, M., van Vuuren, D. P. & Junginger, M. Plastic futures and their CO_2 emissions. *Nature* **612**, 272–276 (2022).
2. Xie, W. et al. Crop switching can enhance environmental sustainability and farmer incomes in China. *Nature* **616**, 300–305 (2023).
3. Deprez, A. et al. Sustainability limits needed for CO_2 removal. *Science* **383**, 484–486 (2024).
4. Cheng, B. H. et al. Bio-coal: a renewable and massively producible fuel from lignocellulosic biomass. *Sci. Adv.* **6**, eaay0748 (2020).
5. Ma, J.-W. et al. A photoluminescent hydrogen-bonded biomass aerogel for sustainable radiative cooling. *Science* **385**, 68–74 (2024).
6. Yuan, P., Sun, Y., Xu, X., Luo, Y. & Hong, M. Towards high-performance sustainable polymers via isomerization-driven irreversible ring-opening polymerization of five-membered thionolactones. *Nat. Chem.* **14**, 294–303 (2021).
7. Cheng, H. et al. Multifaceted applications of cellulosic porous materials in environment, energy, and health. *Prog. Polym. Sci.* **106**, 101253 (2020).
8. Liao, X. et al. Bipolar current collectors of Cu/polymer/Al composite for anode-free batteries. Advanced Functional Materials https://doi.org/10.1002/adfm.202310925 (2024).
9. Maaskant, E. & van Es, D. S. Unexpected susceptibility of poly(-ethylene furanoate) to UV irradiation: a warning light for furandicarboxylic acid?. *ACS Macro Lett.* **10**, 1616–1621 (2021).
10. Yang, K., Dai, J., Zhao, W., Wang, S. & Liu, X. Bio-based epoxy resin demonstrating high breakdown strength and low dielectric loss via intrinsic molecular charge traps construction. *Compos. Part B: Eng.* **284**, 111728 (2024).
11. Zeng, F. et al. Accelerated degradation of PET-based photovoltaic backsheets under UV and acetic acid exposure. *Polymer* **312**, 127671 (2024).
12. Zhang, J. -w, et al. Investigation on the effect of accumulated charge-induced degradation on multilayer photovoltaic insulating backsheets based on atomic force microscopy. *ACS Appl. Energy Mater.* **3**, 8946–8952 (2020).
13. Hornak, J., Kadlec, P., Kopřiva, J. & Polanský, R. Dielectric, structural and mechanical properties of thermally aged biaxially oriented polymeric substrates for flexible electronics. *Polym. Degrad. Stab.* **199**, 109906 (2022).
14. Christmann, J., Gardette, J.-L., Pichon, G., Bouchut, B. & Therias, S. Photostabilization of polyethylene by a hindered amine light stabilizer in blooming conditions and impact of MDO processing. *Polym. Degrad. Stab.* **191**, 109683 (2021).

15. Lu, Y. et al. Interweaved filler network in epoxy resin with reduced interface thermal resistance via in-situ high-temperature "Welding" for significantly improved thermal conductivity. *Chem. Eng. J.* **494**, 153160 (2024).
16. Bi, T.-T. et al. Effect of hydrolysis stabilizers on anti-aging performance of PET under pressure cooker test. *Polym. Degrad. Stab.* **225**, 110816 (2024).
17. Bridson, J. H., Abbel, R., Smith, D. A., Northcott, G. L. & Gaw, S. Impact of accelerated qeathering on the leaching kinetics of stabiliser additives from microplastics. *J. Hazard. Mater.* **459**, 132303 (2023).
18. Böhmer, T. et al. Time reversibility during the ageing of materials. *Nat. Phys.* **20**, 637–645 (2024).
19. Wagermaier, W., Razghandi, K. & Fratzl, P. A bio-inspired perspective on materials sustainability. Adv. Mater. 37, e2413096 (2025).
20. Miao, Y. & Pourquié, O. Modeling human trunk development. *Nat. Biotechnol.* **42**, 1185–1186 (2023).
21. Ma, S. et al. Spatial transcriptomic landscape unveils immunoglobulin-associated senescence as a hallmark of aging. *Cell* **187**, 7025–7044.e7034 (2024).
22. Tidball, J. G. Regulation of muscle growth and regeneration by the immune system. *Nat. Rev. Immunol.* **17**, 165–178 (2017).
23. Fan, L. X., et al. Dual photo-responsive diphenylacetylene enables PET in-situ upcycling with reverse enhanced UV-resistance and strength. *Angew. Chem. Int. Ed.* **62**, e202314448 (2023).
24. Posz, J. M. et al. Synthesis of borylated carbocycles by [2 + 2]-cycloadditions and photo-ene reactions. *J. Am. Chem. Soc.* **146**, 10142–10149 (2024).
25. Xu, C. et al. Soy protein adhesive with bio-based epoxidized daidzein for high strength and mildew resistance. *Chem. Eng. J.* **390**, 124622 (2020).
26. Li, X.-L. et al. A synchronously chemically closed-loop and high-performance approach for furan-based copolyesters with robustness, high gas barriers, and high puncture resistance. *Green. Chem.* **24**, 8552–8561 (2022).
27. Li, Z.-M. et al. High-performance chemically recyclable multifunctional polyolefin-like biomass-derived polyester materials. *Mater. Horiz.* **12**, 946–956 (2025).
28. Van Geem, K. M. Waste recycling is gaining momentum. *Science* **381**, 607–608 (2023).
29. Ding, J. et al. Flexible and recyclable bio-based polyester composite films with outstanding mechanical and gas barrier properties using leaf-shaped CNT@BNNS covalent heterojunction. *Small* **20**, 2406958 (2024).
30. Christensen, P. R., Scheuermann, A. M., Loeffler, K. E. & Helms, B. A. Closed-loop recycling of plastics enabled by dynamic covalent diketoenamine bonds. *Nat. Chem.* **11**, 442–448 (2019).
31. Korley, L. T. J., Epps, T. H., Helms, B. A. & Ryan, A. J. Toward polymer upcycling—adding value and tackling circularity. *Science* **373**, 66–69 (2021).
32. Kagawa, H. et al. Human blastoids model blastocyst development and implantation. *Nature* **601**, 600–605 (2021).
33. Matsuda, T., Kawakami, R., Namba, R., Nakajima, T. & Gong, J. P. Mechanoresponsive self-growing hydrogels inspired by muscle training. *Science* **363**, 504–508 (2019).
34. Cai, W. et al. Force-induced transition of π–π stacking in a single polystyrene chain. *J. Am. Chem. Soc.* **141**, 9500–9503 (2019).
35. Li, X. L. et al. A multifunctional bio-based polyester material integrated with high mechanical performance, gas barrier performance, and chemically closed-loop. *Adv. Funct. Mater.* **34**, 2400911 (2024).
36. Xie, K., Li, Z., Zhao, B., Guo, Z. & Deng, X. Construction of fluorenyl-modified low dielectric constant polyimide films with excellent mechanical properties and optical transparency. *J. Appl. Polym. Sci.* **141**, e55217 (2024).
37. Ishida, T., Kitagaki, R., Hagihara, H. & Elakneswaran, Y. Role of moisture in photo-ageing -macromolecular architecture evolution of acrylic-urethane network. *Polym. Test.* **96**, 107123 (2021).
38. Mane, P., Keche, A. J., Chopra, S. & Pande, K. Effect of polycarbonate (PC) content on the mechanical properties, morphology and transesterification mechanism of PBT/PC immiscible blends. *J. Appl. Polym. Sci.* **141**, e55902 (2024).
39. Wu, Y. et al. Multiple-functional molecularly imprinted nanocomposite membranes for high-efficiency selective separation applications: an imitated core-shell TiO2@PDA-based MIMs design. *Compos. Part B: Eng.* **198**, 108123 (2020).
40. Sit, S., Chakraborty, G. & Das, N. C. Superior EMI shielding effectiveness with enhanced electrical conductivity at low percolation threshold of flexible novel ethylene methyl acrylate/single-walled carbon nanotube nanocomposites. *Polym. Eng. Sci.* **62**, 2047–2060 (2022).
41. Nikbakht Nasrabadi, M., Sedaghat Doost, A. & Mezzenga, R. Modification approaches of plant-based proteins to improve their techno-functionality and use in food products. *Food Hydrocoll.* **118**, 106789 (2021).
42. Liang, Y. et al. Municipal sewage sludge incineration and its air pollution control. *J. Clean. Prod.* **295**, 126456 (2021).
43. Wang, S. et al. Theoretical modeling and experimental verification of percolation threshold with MWCNTs' rotation and translation around a growing bubble in conductive polymer composite foams. *Compos. Sci. Technol.* **199**, 108345 (2020).
44. Garrell, M. G., Ma, B.-M., Shih, A. J., Lara-Curzio, E. & Scattergood, R. O. Mechanical properties of polyphenylene-sulfide (PPS) bonded Nd–Fe–B permanent magnets. *Mater. Sci. Eng.: A* **359**, 375–383 (2003).
45. Burgess, S. K. et al. Chain mobility, thermal, and mechanical properties of poly(ethylene furanoate) compared to poly(ethylene terephthalate). *Macromolecules* **47**, 1383–1391 (2014).
46. Marangoni Junior, L. et al. High-pressure processing effects on the barrier properties of flexible packaging materials. *J. Food Process. Preserv.* **44**, e14865 (2020).
47. Jagannath, J., Nadanasabapathi, S. & Bawa, A. Effect of starch on thermal, mechanical, and barrier properties of low-density polyethylene film. *J. Appl. Polym. Sci.* **99**, 3355–3364 (2006).
48. Salehi, A., Jafari, S. H., Khonakdar, H. A. & Ebadi-Dehaghani, H. Temperature dependency of gas barrier properties of biodegradable PP/PLA/nanoclay films: experimental analyses with a molecular dynamics simulation approach. *J. Appl. Polym. Sci.* **135**, 108345 (2018).
49. Yi, J. et al. Development of a series of biobased poly(ethylene 2,5-furandicarboxylate-co-(5,5′-((phenethylazanediyl)bis(methylene)) bis(furan-5,2-diyl))dimethylene 2,5-furandicarboxylate) copolymers via a sustainable and mild route: promising "breathing" food packaging materials. *Green. Chem.* **24**, 5181–5190 (2022).
50. Hu, H. et al. A mild method to prepare high molecular weight poly (butylene furandicarboxylate-co-glycolate) copolyesters: effects of the glycolate content on thermal, mechanical, and barrier properties and biodegradability. *Green. Chem.* **21**, 3013–3022 (2019).
51. Wang, R. et al. Scientific discovery framework accelerating advanced polymeric materials design. *Research* **7**, 0406 (2024).
52. Zha, J.-W. et al. Polymer dielectrics for high-temperature energy storage: constructing carrier traps. *Prog. Mater. Sci.* **140**, 101208 (2023).
53. Yuan, C. et al. Polymer/molecular semiconductor all-organic composites for high-temperature dielectric energy storage. *Nat. Commun.* **11**, 3919 (2020).
54. Wörner, H. J. et al. Charge migration and charge transfer in molecular systems. *Struct. Dyn.* **4**, 061508 (2017).

55. Huang, B. et al. Improving charge storage of biaxially-oriented polypropylene under extreme electric fields by excimer UV irradiation. *Adv. Mater.* **36**, 2311713 (2024).
56. Chen, N., Du, B., Ding, J. & Zhang, G.- Thermoplastic environmentally friendly insulating material: self-assembled insulating film supporting water repellent effect. 831-838 (2024).
57. Tiankai, J., Jun, Z., Wei, H. & Keda, Z. Fabrication life prediction model for HDPE/Cr2O3 composites toward roof passive cooling. *Constr. Build. Mater.* **369**, 130495 (2023).
58. Hu, Q. et al. Anti-UV and hydrophobic dual-functional coating fabrication for flame-retardant polyester fabrics by surface-initiated PET RAFT technique. *Eur. Polym. J.* **173**, 111275 (2022).
59. Blumthaler, M. UV Monitoring for public health. *Int. J. Environ. Res. Public Health* **15**, 1723 (2018).
60. Quinn, E. C. et al. Installing controlled stereo-defects yields semicrystalline and biodegradable poly(3-Hydroxybutyrate) with high toughness and optical clarity. *J. Am. Chem. Soc.* **5795**, 5802 (2023).
61. Zhou, L. et al. Chemically circular, mechanically tough, and melt-processable polyhydroxyalkanoates. *Science* **380**, 64–69 (2023).
62. Zhao, T.-H., Yuan, W.-Q., Li, Y.-D., Weng, Y.-X. & Zeng, J.-B. Relating chemical structure to toughness via morphology control in fully sustainable sebacic acid cured epoxidized soybean oil toughened polylactide blends. *Macromolecules* 2027–2037 (2018).
63. Hillmyer, M. A. The promise of plastics from plants. *Science* **358**, 868–870 (2017).
64. Jiang, Y. et al. Upcycling heteroatom-containing plastics via bimetallic synergistic catalysis: Unveiling the role of O and Cl in C-H bond cleavage. *Chemical Engineering Journal* https://doi.org/10.1016/j.cej.2024.153169 (2024).
65. Liu, Y., et al. Covalent adaptable polyester networks based on citric acid with fast dynamic behaviors and closed-loop recyclability. ACS Macro Lett. 14, 917–924 (2025).
66. Zhu, H. et al. Design of environmentally degradable polyethylene-like polyesters and eco-friendly recycling via commercial enzymes. *Green. Chem.* **27**, 6660–6675 (2025).
67. Cai, X. et al. A sustainable poly(butylene furandicarboxylate) (PBF)-based copolyester containing a cyclic ether structure: integrated with high thermal, mechanical, and hydrolytic degradable properties. *ACS Sustain. Chem. Eng.* **13**, 658–668 (2025).
68. Kainulainen, T. P. et al. Furan-based polyesters from diethylene glycol with facile chemical recyclability. *Macromolecules* **58**, 4160–4169 (2025).
69. Li, S. et al. A novel hydroxyl-rich polyvinyl alcohol hot-melt adhesive with excellent ultra-low temperature adhesion and reusability. *J. Appl. Polym. Sci.* **141**, e55613 (2024).

Acknowledgments

This work was supported by the National Natural Science Foundation of China (22375138), the State Key Laboratory of Advanced Polymer Materials (Grant No. sklpme2024-2-02), the 111 Project (B20001), the Institutional Research Fund from Sichuan University (2021SCUNL201), and the Fundamental Research Funds for the Central Universities (granted to T. Fu). It was also supported by the National Natural Science Foundation of China (52403014, awarded to X. L. Li).

Author contributions

T. Fu and X. L. Li conceived of the project and designed the research. R. Z. Wu supervised by X. L. Li, X. L. Wang, Y .Z. Wang and T. Fu performed most of the experiments and drafting of the paper. H. S. Cai designed the chemical recycling strategy. N. Zhao, F. G. Wang, and K. R. Ye assisted in the synthesis and characterization of the polymer. All authors contributed to editing the paper.

Competing interests

The authors declare no competing interests.

Additional information

Supplementary information The online version contains supplementary material available at https://doi.org/10.1038/s41467-025-64664-9.

Correspondence and requests for materials should be addressed to Xing-Liang Li or Teng Fu.

Peer review information *Nature Communications* thanks Jinggang Wang, and the other, anonymous, reviewer(s) for their contribution to the peer review of this work. A peer review file is available.